^{77}Se Solid-State NMR Studies of $[M(Se_4)_2]^{2-}$ Anions (M = Zn, Cd, Hg)

Patrick J. Barrie, Robin J. H. Clark,* and Robert Withnall†

Christopher Ingold Laboratories, University College London, 20 Gordon Street, London WC1H 0AJ, U.K.

Duck-Young Chung, Kang-Woo Kim, and Mercouri G. Kanatzidis

Department of Chemistry, Michigan State University, East Lansing, Michigan 48824

Received September 22, 1993⊛

^{77}Se solid-state NMR spectra have been recorded with cross-polarization and magic-angle spinning on $[M(Se_4)_2]^{2-}$ complexes with $[Me_4N]^+$ (M = Zn, Cd, Hg) and $[Et_4N]^+$ (M = Cd, Hg). The large chemical shift anisotropies (of the order of 1000 ppm) mean that fast spinning speeds (9–11 kHz) are needed in order to reveal the number of crystallographic selenium sites present within the solid. The spectra enable the principal components of the ^{77}Se shielding tensor to be calculated from the spinning sideband intensities. Differences between the ^{77}Se isotropic chemical shifts observed for the $[Et_4N]^+$ complexes and for the $[Me_4N]^+$ complexes reflect small structural changes in the $[M(Se_4)_2]^{2-}$ geometry with cation. *J*-coupling to ^{199}Hg and $^{111/113}Cd$ are also observed. The solid-state NMR results are compared with similar work in solution. A single-crystal X-ray structure determination of $[Me_4N]_2[Hg(Se_4)_2]\cdot 0.5DMF$ is reported (monoclinic crystal system, space group $C2/c$). The Hg atom is tetrahedrally coordinated by two chelating tetraselenide ligands with both $HgSe_4$ rings adopting the envelope conformation. The FT Raman spectrum of $[Me_4N]_2[Cd(Se_4)_2]$ is also reported.

Introduction

There has been significant research interest recently in the chemistry of metal polyselenides and polytellurides due to the extensive range of complexes with novel and interesting structures that can be formed.[1,2] Thus far, characterization of these complexes has depended principally on single-crystal X-ray diffraction studies, though there has been a certain amount of $^{77}Se/^{125}Te$ NMR work on these species in solution.[2] In this paper we report high-resolution solid-state ^{77}Se NMR results on $[M(Se_4)_2]^{2-}$ complexes with $[Me_4N]^+$ (M = Zn, Cd, Hg) and $[Et_4N]^+$ (M = Cd, Hg) (DMF solvates in each case; DMF = dimethylformamide). Solution NMR results on some $[M(Se_4)_2]^{2-}$ complexes have been reported previously by Ansari *et al.*[3] Recording the spectra in the solid state has the advantage that it slows down any fluxional processes that may occur in solution and allows direct comparison between NMR chemical shifts and the crystal structure. It has the added advantage that it can provide a measure of the anisotropy of the shielding tensor, which is in general a more sensitive probe of local geometry than is the isotropic chemical shift measured in solution. There have thus far been very few published ^{77}Se solid-state NMR studies,[4-7] and this is the first report of solid-state NMR results on polyselenide complexes. It is anticipated that the results on these model compounds will prove useful in recording and interpreting ^{77}Se NMR spectra of new polychalcogenide solids.[8] Also included in this paper are the results of an X-ray crystallographic study of $[Me_4N]_2[Hg(Se_4)_2]\cdot 0.5DMF$, since this proved to be relevant to the interpretation of the solid-state NMR spectra of this and related complexes, and brief comments on the FT Raman spectra of the complexes.

Experimental Section

Syntheses. $[Me_4N]_2[Hg(Se_4)_2]\cdot 0.5DMF$ was prepared by the following method.[9] To a 50-cm^3 DMF solution of 0.53 g (1.5 mmol) of Na_2Se_4 and 0.16 g (1.5 mmol) of $[Me_4N]Cl$ was added dropwise for 15 min a 10 cm^3 DMF solution of 0.20 g (0.74 mmol) of $HgCl_2$, resulting in a dark reddish brown solution. After removal of undissolved precipitates by filtration, 60 cm^3 of ether was slowly layered over the filtrate solution to yield, in 1 day, reddish black chunky crystals. These crystals were isolated and washed with ether several times. More crystals were obtained upon layering an additional 30 cm^3 of ether over the filtrate solution. Overall yield: 54%. Quantitative microprobe analyses of the complexes were performed on a JEOL 35CF scanning electron microscope (SEM) equipped with a Tracor Northern TN 5500 X-ray microanalysis attachment. Single crystals were mounted on an aluminum stub using conducting silver paint to help dissipate charges that develop on the sample surface during the measurement of energy dispersive spectra (EDS). A correction factor was applied to the analyses based on EDS results on compounds of known chemical composition. The analyses were an average of four to six individual measurements on different crystals of each compound. The chemical composition of $[Me_4N]_2[Hg(Se_4)_2]\cdot 0.5DMF$ determined by this method showed a Hg:Se ratio of 1:6.9. The density of the crystals was measured to be 2.66 g cm^{-3} using a mixture of $CHBr_3$ and *n*-heptane.

The syntheses of $[Me_4N]_2[M(Se_4)_2]$ (M = Cd, Zn) and $[Et_4N]_2[M(Se_4)_2]$ (M = Hg, Cd) were accomplished by following the same procedure as above, using the appropriate metal chlorides and $[Me_4N]Cl$ or $[Et_4N]Br$ salts. All samples were stored under nitrogen prior to the NMR measurements.

Crystallography. A single crystal of $[Me_4N]_2[Hg(Se_4)_2]\cdot 0.5DMF$[9] was placed inside a glass capillary and sealed in using a flame. The crystallographic data were collected on a Nicolet P3 four-circle automated

† Current address: University of Greenwich, Wellington St., Woolwich, London SE18 6PF, U.K.

⊛ Abstract published in *Advance ACS Abstracts,* February 15, 1994.

(1) (a) Roof, L. C.; Kolis, J. W. *Chem. Rev.* **1993**, *93*, 1037. (b) Huang, S.-P.; Kanatzidis, M. G. *Coord. Chem. Rev.*, in press.
(2) (a) Kanatzidis, M. G. *Comments Inorg. Chem.* **1990**, *10*, 161. (b) Ansari, M. A.; Ibers, J. A. *Coord. Chem. Rev.* **1990**, *100*, 223.
(3) Ansari, M. A.; Mahler, C. H.; Chorghade, G. S.; Lu, Y.-J.; Ibers, J. A. *Inorg. Chem.* **1990**, *29*, 3832.
(4) Collins, M. J.; Ratcliffe, C. I.; Ripmeester, J. A. *J. Magn. Reson.* **1986**, *68*, 172.
(5) Harris, R. K.; Sebald, A. *Magn. Reson. Chem.* **1987**, *25*, 1058.
(6) Gay, I. D.; Jones, C. H. W.; Sharma, R. D. *J. Magn. Reson.* **1989**, *84*, 501.
(7) Batchelor, R. J.; Einstein, F. W. B.; Gay, I. D.; Gu, J.-H.; Pinto, B. M. *J. Organomet. Chem.* **1991**, *411*, 147.
(8) Kanatzidis, M. G. *Chem. Mater.* **1990**, *2*, 353.
(9) The DMF-free $[Me_4N]_2[Hg(Se_4)_2]$ was also prepared and structurally characterized. It crystallizes in the orthorhombic space group *Pbca* (No. 61) with a = 15.898(2) Å, b = 15.321(2) Å, c = 18.523(3) Å, V = 4512(1) Å^3, and Z = 8.

0020-1669/94/1333-1212$04.50/0

Table 1. Crystallographic Data for $[Me_4N]_2[Hg(Se_4)_2]\cdot 0.5DMF$

formula	$C_{10.5}H_{27.5}N_{2.5}O_{0.5}HgSe_8$	fw	1017.11
a/Å	33.722(10)	space group	$C2/c$ (No. 15)
b/Å	10.658(3)	T/°C	23
c/Å	13.961(3)	λ/Å	0.710 73
β/deg	98.05(2)	ρ_{calc}/g cm^{-3}	2.719
V/Å^3	4969(2)	ρ_{obs}/g cm^{-3}	2.66
Z	8	μ/cm^{-1}	178.0
R/R_w[a]	0.060/0.061		

[a] $R = \Sigma||F_o| - |F_c||/\Sigma|F_o|$; $R_w = [\Sigma w(|F_o| - |F_c|)^2/\Sigma w|F_o|^2]^{1/2}$.

Table 2. Fractional Atomic Coordinates and B_{eq} Values for Non-Hydrogen Atoms in $[Me_4N]_2[Hg(Se_4)_2]\cdot 0.5DMF$ with Their Estimated Standard Deviations in Parentheses

atom	x	y	z	B_{eq}/Å^2 [a]
Hg(1)	0.36676(3)	0.0640(1)	0.60318(9)	3.44(6)
Se(1)	0.32867(8)	−0.0586(3)	0.4500(2)	3.8(1)
Se(2)	0.3073(1)	−0.2324(3)	0.5324(3)	4.5(2)
Se(3)	0.3612(1)	−0.2694(3)	0.6543(2)	4.0(2)
Se(4)	0.36151(9)	−0.0875(3)	0.7476(2)	3.9(2)
Se(5)	0.33571(9)	0.2901(3)	0.6320(2)	3.9(2)
Se(6)	0.3885(1)	0.4178(3)	0.6033(2)	4.7(2)
Se(7)	0.4155(1)	0.3099(4)	0.4824(3)	5.1(2)
Se(8)	0.43782(8)	0.1252(3)	0.5582(2)	4.2(2)
O(1)	$^1/_2$	0.420(6)	$^1/_4$	16(1)
N(1)	0.2245(6)	0.098(2)	0.655(2)	4(1)
N(2)	0.0592(6)	0.219(2)	0.098(2)	4(1)
N(3)	$^1/_2$	0.227(4)	$^1/_4$	5.1(9)
C(1)	0.246(1)	0.059(3)	0.573(3)	5.7(8)
C(2)	0.214(1)	0.233(4)	0.641(3)	8(1)
C(3)	0.250(1)	0.083(5)	0.746(4)	11(1)
C(4)	0.186(1)	0.032(4)	0.647(3)	8(1)
C(5)	0.1009(8)	0.168(3)	0.114(2)	4.7(7)
C(6)	0.031(1)	0.133(5)	0.138(3)	10(1)
C(7)	0.057(2)	0.339(6)	0.139(4)	14(2)
C(8)	0.045(1)	0.237(5)	−0.003(4)	11(1)
C(9)	0.529(2)	0.299(7)	0.232(5)	6(1)
C(10)	0.525(1)	0.116(8)	0.217(6)	22(1)

[a] Anisotropically refined atoms are given in the form of the isotropic equivalent displacement parameter defined as $B_{eq} = (8\pi^2/3)[a^2B_{11} + b^2B_{22} + c^2B_{33} + ab(\cos\gamma)B_{12} + ac(\cos\beta)B_{13} + bc(\cos\alpha)B_{23}]$. The anisotropic temperature factor expression is $\exp[-2\pi^2(B_{11}a^{*2}h^2 + \ldots + 2B_{12}a^*b^*hk + \ldots)]$.

diffractometer. Accurate unit cell parameters were determined from the $2\theta, \omega, \phi$, and χ angles of 25 machine-centered reflections. The intensities of three standard reflections were checked every 100 reflections to monitor crystal and instrument stability. No serious decay was observed during the data collection period. An empirical absorption correction based on ψ scans of three strong reflections with $\chi \sim 90°$ was applied to the data set. The structures were solved by direct methods using the SHELXS-86 software program and refined with full-matrix least-squares techniques. After isotropic refinement of all atoms, a DIFABS correction was applied.[10] All calculations were performed on a VAX station 3100/76 computer using the TEXSAN crystallographic software package of the Molecular Structure Corp.[11] All atoms in the $[Hg(Se_4)_2]^{2-}$ anion were refined anisotropically. The N atoms of the $[Me_4N]^+$ cations were refined anisotropically, but the C atoms were refined isotropically. All non-hydrogen atoms in the DMF molecule were refined isotropically. The hydrogen atom positions were calculated, but not refined. The O(1) and N(3) atoms of DMF are sitting on a 2-fold axis ($^1/_2, y, ^1/_4$) and the C(9) atoms are disordered between two positions generated by the 2-fold axis ($^1/_2, y, ^1/_4$) with a half occupancy. Table 1 shows the crystal data and details of the structure analysis. The fractional coordinates and temperature factors (B_{eq}) of all atoms with their estimated standard deviations are given in Table 2.

Solid-State NMR. The solid-state NMR spectra were recorded with a multinuclear Bruker MSL-300 spectrometer using cross-polarization (CP), magic-angle spinning (MAS), and high-power proton decoupling. The spectra were recorded using three different spinning speeds in the range 9–11 kHz in order to identify unambiguously the isotropic resonance positions. The CP match condition was set on solid ammonium selenate, which was also used as an external secondary reference taken to resonate at 1040.2 ppm from Me_2Se.[4] A contact time of 12 ms was used for the $[Me_4N]^+$ complexes, and 4 ms was used for the $[Et_4N]^+$ complexes. The recycle delay between scans was 1–3 s. Spinning sideband intensities were simulated using the method of Herzfeld and Berger[12] to give the principal components of the shielding tensor (σ_{11}, σ_{22}, and σ_{33}). The σ values are quoted as shieldings, rather than as chemical shifts which have the opposite sign, using the convention $|\sigma_{33} - \sigma_{iso}| > |\sigma_{11} - \sigma_{iso}| > |\sigma_{22} - \sigma_{iso}|$. The anisotropy $\Delta\sigma$ is defined as $\sigma_{33} - 0.5(\sigma_{11} + \sigma_{22})$, and the asymmetry parameter, η, by $(\sigma_{22} - \sigma_{11})/(\sigma_{33} - \sigma_{iso})$, where $\sigma_{iso} = -\delta_{iso} = (\sigma_{11} + \sigma_{22} + \sigma_{33})/3$.

FT Raman Spectra. FT Raman spectra of the complexes were obtained from powdered solids at room temperature using a Nicolet 910 FT Raman spectrometer equipped with a Nd/YAG laser emitting at 1064 nm and a liquid-nitrogen-cooled germanium detector. The spectral resolution was 4 cm^{-1}, and the laser power at the sample was approximately 70 mW.

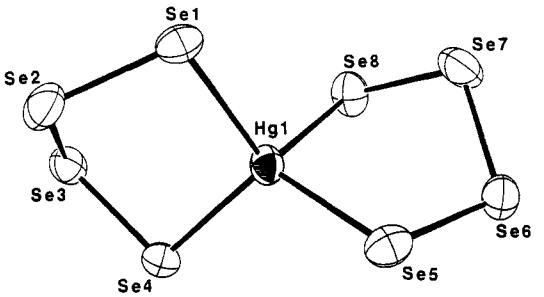

Figure 1. Structure of $[Hg(Se_4)_2]^{2-}$ anion in $[Me_4N]_2[Hg(Se_4)_2]\cdot 0.5DMF$.

Results

Figure 1 shows the structure of the $[Hg(Se_4)_2]^{2-}$ anion in $[Me_4N]_2[Hg(Se_4)_2]\cdot 0.5DMF$, which is essentially the same as that of the $[Na(15\text{-crown-}5)]^+$ and $[Ph_4P]^+$ salts.[13,14] The Hg atom is tetrahedrally coordinated by two chelating tetraselenide ligands, and all eight selenium atoms occupy distinct crystallographic sites. Both $HgSe_4$ rings in $[Hg(Se_4)_2]^{2-}$ exhibit the envelope conformation. The Hg(1), Se(1), Se(2), and Se(4) atoms are in a plane with a mean deviation of 0.03(2) Å, and the Se(3) atom lies 1.27 Å below it. Similarly, the Hg(1), Se(5), Se(6), and Se(8) atoms are in a plane with a mean deviation of 0.005(3) Å, while the Se(7) atom lies 1.27 Å above it. The dihedral angle between the two least-squares planes is 84.33°.

Selected bond distances and angles in the $[Hg(Se_4)_2]^{2-}$ anion are summarized in Table 3. The average Hg–Se and Se–Se distances in this complex are 2.65(3) and 2.33(1) Å, respectively. These distances are almost the same as those found for complexes in which the $[Hg(Se_4)_2]^{2-}$ anion is balanced by much larger cations such as $[Na(15\text{-crown-}5)]^+$ and $[Ph_4P]^+$.[13,14] Interestingly, there is little structural shrinkage or distortion of the $[Hg(Se_4)_2]^{2-}$ anion caused by the presence of the smaller $[Me_4N]^+$ cation. The distortion of Se(3) and Se(7) out of the plane and the fact that the Hg–Se(4) and Hg–Se(8) distances are appreciably shorter than the other two Hg–Se bond distances may be a result of crystal packing forces. It may also be relevant that Se(4) has only one hydrogen within 3.35 Å, while the other Hg-bonded Se atoms have more. The closest intermolecular Se–Se distances are 3.537(5) Å. Figure 2 shows the packing diagram of $[Me_4N]_2[Hg(Se_4)_2]\cdot 0.5DMF$ in the unit cell. Pertinent to the solid-state NMR results reported below, Figure 3 shows the H atom environments around the $[Hg(Se_4)_2]^{2-}$ anion. Distances with a Se---H length of less than the sum of the van der Waals radii[15]

(10) Walker, N.; Stuart, D. DIFABS: An Empirical Method for Correcting Diffractometer Data for Absorption Effects. *Acta Crystallogr.* **1983**, *A39*, 158.
(11) TEXSAN: Single Crystal Structure Analysis Software, Version 5.0, Molecular Structure Corp., The Woodlands, TX.
(12) Herzfeld, J.; Berger, A. E. *J. Chem. Phys.* **1980**, *73*, 6021.
(13) Adel, J.; Weller, F.; Dehnicke, K. *Z. Naturforsch.* **1988**, *43B*, 1094.
(14) Banda, R. M. H.; Cusick, J.; Scudder, M. L.; Craig, D. C.; Dance, I. G. *Polyhedron* **1989**, *8*, 1995.
(15) Huheey, J. E. *Inorganic Chemistry*, 3rd ed.; Harper & Row: New York, 1983; pp 258–259.

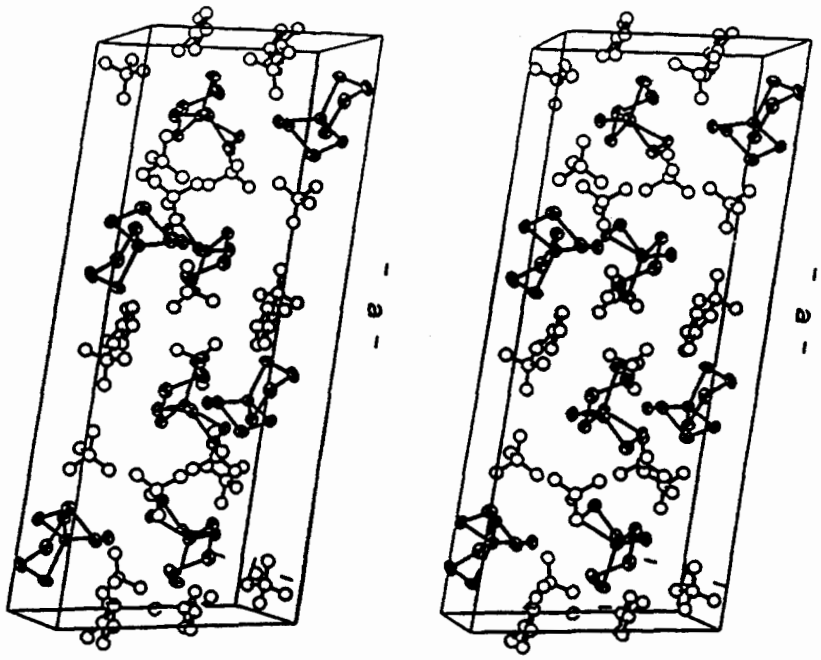

Figure 2. Packing diagram of $[Me_4N]_2[Hg(Se_4)_2]\cdot 0.5DMF$ in the unit cell.

Table 3. Selected Bond Distances (Å) and Angles (deg) in the $[Hg(Se_4)_2]^{2-}$ Anion of $[Me_4N]_2[Hg(Se_4)_2]\cdot 0.5DMF$[a]

Hg(1)–Se(1)	2.677(3)	Se(1)–Se(2)	2.347(5)
Hg(1)–Se(4)	2.609(3)	Se(2)–Se(3)	2.344(5)
Hg(1)–Se(5)	2.680(3)	Se(3)–Se(4)	2.335(5)
Hg(1)–Se(8)	2.642(3)	Se(5)–Se(6)	2.320(5)
		Se(6)–Se(7)	2.330(5)
		Se(7)–Se(8)	2.311(5)
Hg–Se (mean)	2.65(3)	Se–Se (mean)	2.33(1)
Se(1)–Hg(1)–Se(4)	103.8(1)	Hg(1)–Se(1)–Se(2)	98.0(1)
Se(1)–Hg(1)–Se(5)	113.9(1)	Hg(1)–Se(4)–Se(3)	94.5(1)
Se(1)–Hg(1)–Se(8)	106.3(1)	Hg(1)–Se(5)–Se(6)	100.1(1)
Se(4)–Hg(1)–Se(5)	111.7(1)	Hg(1)–Se(8)–Se(7)	94.1(1)
Se(4)–Hg(1)–Se(8)	119.9(1)	Se(1)–Se(2)–Se(3)	103.2(1)
Se(5)–Hg(1)–Se(8)	101.5(1)	Se(2)–Se(3)–Se(4)	102.0(2)
		Se(5)–Se(6)–Se(7)	102.9(2)
		Se(6)–Se(7)–Se(8)	102.9(2)

[a] The estimated standard deviations in the mean bond distances were calculated by the equation $\sigma_1 = [\sum n(l_n - l)^2/n(n-1)]^{1/2}$, where l_n is the distance of the nth bond, l is the mean bond distance, and n is the number of bonds.

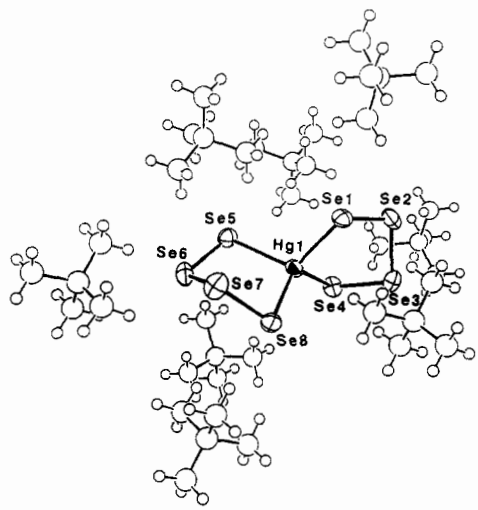

Figure 3. Cation and DMF environments around the $[Hg(Se_4)_2]^{2-}$ anion in $[Me_4N]_2[Hg(Se_4)_2]\cdot 0.5DMF$.

Table 4. Selected Bond Distances (<3.35 Å) between Se and H Atoms in $[Me_4N]_2[Hg(Se_4)_2]\cdot 0.5DMF$

Se(1)–H(15)	2.997	Se(5)–H(2)	3.142
Se(1)–H(8)	3.273	Se(5)–H(8)	3.256
Se(1)–H(1)	3.321	Se(6)–H(13)	3.094
Se(1)–H(3)	3.343	Se(6)–H(11)	3.095
Se(2)–H(1)	2.973	Se(6)–H(14)	3.192
Se(2)–H(15)	3.269	Se(7)–H(14)	3.162
Se(3)–H(10)	3.063	Se(7)–H(11)	3.321
Se(3)–H(6)	3.175	Se(8)–H(21)	3.132
Se(4)–H(6)	2.820	Se(8)–H(22)	3.197
Se(5)–H(3)	2.981	Se(8)–H(16)	3.220
Se(5)–H(5)	3.021	Se(8)–H(20)	3.345
Se(5)–H(13)	3.068		

of the H and Se atoms, 3.35 Å, are shown in Table 4. The shortest Se---H intermolecular contact is 2.820 Å.

The ^{77}Se CP/MAS NMR spectrum of $[NMe_4]_2[Hg(Se_4)_2]$ at a spinning speed of 10 670 Hz is shown in Figure 4. Despite the high spinning speed used, an extensive array of spinning sidebands is observed which is indicative of sites with a high chemical shift anisotropy. By recording the spectra at two other spinning speeds, we established unambiguously the positions of eight isotropic resonance peaks (A–H), and these peaks correspond to the eight distinct selenium sites within the crystal. It should be pointed out that the spectral complexity and degree of overlap between the spinning sideband arrays from each site meant that it was impossible to analyze spectra recorded at the more conventional MAS spinning speeds of *ca.* 5 kHz.

The four sites resonating at higher field (peaks E–H) show additional satellites, each having intensity of *ca.* 8% of that of the central peak, due to indirect (J-) coupling between ^{77}Se and ^{199}Hg (which has spin $I = {}^1/_2$ and a natural abundance of 16.8%). The $^1J(^{77}Se–^{199}Hg)$ values are in the range 1220–1480 Hz, which indicates that these peaks correspond to the environments in which selenium atoms are directly bonded to a mercury atom. Close examination of the base of the other four peaks (those due to selenium atoms in the rings) indicates that three of these show barely resolved weak J-coupling satellites (with $J \sim 330$ Hz) which are probably due to a two-bond coupling to ^{199}Hg. There is also the possibility that these peaks might result from coupling between ^{77}Se nuclei, though such a coupling would be expected to be only *ca.* 160 Hz (see below). The other peak (peak D) is slightly broader than the others (with a peak width at half-height of 180 Hz compared to 85 Hz for the others), and so this weaker coupling is not visible. The spinning sideband intensities of the

Table 5. Summary of ^{77}Se Solid-State NMR Results on $[Me_4N]_2[Hg(Se_4)_2]$

	δ_{iso}/ppm	σ_{11}/ppm	σ_{22}/ppm	σ_{33}/ppm	$\Delta\sigma$/ppm	η	J_{Se-Hg}/Hz
A	693.4	−1246	−849	+15	1062(±80)	0.56(±0.10)	330(±50)
B	634.0	−1086	−828	+12	969(±30)	0.40(±0.04)	330(±50)
C	619.4	−1089	−740	−29	885(±50)	0.59(±0.16)	330(±50)
D	527.4	−1050	−666	+135	993(±80)	0.58(±0.10)	
E	101.4	−591	−111	+398	749(±20)	0.96(±0.04)	1220(±30)
F	89.9	+419	−77	−612	−783(±20)	0.95(±0.03)	1290(±30)
G	47.7	−581	−76	+514	843(±30)	0.90(±0.05)	1360(±30)
H	30.2	−552	−82	+543	860(±30)	0.82(±0.05)	1480(±30)

Table 6. Summary of ^{77}Se Solid-State NMR Results on $[Me_4N]_2[Zn(Se_4)_2]$[a]

	δ_{iso}/ppm	σ_{11}/ppm	σ_{22}/ppm	σ_{33}/ppm	$\Delta\sigma$/ppm	η	J_{Se-Se}/Hz
A	670.3	−1068	−914	−29	962(±80)	0.24(±0.10)	150(±30)
B	656.7	−1044	−899	−27	945(±90)	0.23(±0.12)	150(±30)
C	637.2	−1048	−809	−55	874(±50)	0.41(±0.07)	170(±30)
D	595.3	−1046	−704	−36	839(±50)	0.61(±0.08)	150(±30)
E	71.0	−600	−93	+480	827(±50)	0.92(±0.08)	150(±30)
F	121.6	−657	−135	+428	824(±50)	0.95(±0.08)	180(±30)
G	136.8	+379	−16	−773	−955(±70)	0.62(±0.09)	170(±30)
H	142.2	−593	−184	+350	739(±30)	0.83(±0.06)	150(±30)

[a] The sample also contained a small amount of impurity which had isotropic resonances at 890.7, 464.2, and 663.0 ppm.

Table 7. Summary of ^{77}Se Solid-State NMR Results on $[Me_4N]_2[Cd(Se_4)_2]$[a]

	δ_{iso}/ppm	σ_{11}/ppm	σ_{22}/ppm	σ_{33}/ppm	$\Delta\sigma$/ppm	η	J_{Se-Cd}/Hz
A	662.4	−1052	−922	−13	973(±100)	0.20(±0.14)	
B	641.5	−1063	−856	−6	954(±90)	0.32(±0.11)	
C	611.3	−973	−874	+14	937(±90)	0.16(±0.14)	
D	599.9	−952	−799	−49	826(±80)	0.28(±0.12)	
E	63.0	+490	+60	−739	−1014(±60)	0.64(±0.08)	250(±30)
F	70.7	+571	+11	−794	−1085(±100)	0.77(±0.15)	330(±30)
G	92.3	+519	−37	−759	−999(±70)	0.83(±0.11)	290(±30)
H	127.5	+501	−57	−827	−1050(±70)	0.80(±0.08)	290(±30)

[a] The sample also contained a small amount of impurity which had isotropic resonances at 681.7, 635.9, 631.1, 547.4, 19.9, and 7.5 ppm.

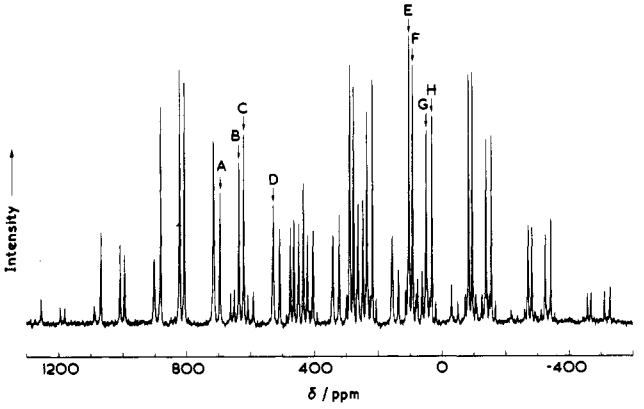

Figure 4. ^{77}Se CP/MAS NMR spectrum of $[Me_4N]_2[Hg(Se_4)_2]$. The isotropic peaks are marked, while the other peaks are spinning sidebands (spinning speed = 10 670 Hz).

spectra obtained were analyzed, and the results, including estimated uncertainties in $\Delta\sigma$ and η, are summarised in Table 5.

High-quality CP/MAS NMR spectra were also obtained on $[Me_4N]_2[Zn(Se_4)_2]$ and $[Me_4N]_2[Cd(Se_4)_2]$. The results, including the principal components of the shielding tensor, are given in Tables 6 and 7. The exact structures of these compounds are not known. They give powder X-ray diffraction patterns similar but not identical to those for $[Me_4N]_2[Hg(Se_4)_2]$. Their structures are thus expected to be closely related, but not completely isostructural. The CP/MAS NMR spectra of both samples show eight isotropic resonances, indicating that, as in the case of $[Me_4N]_2[Hg(Se_4)_2]$, the selenium atoms in both complexes all occupy crystallographically distinct sites in the unit cell. This situation may be contrasted with that implied by the crystal structure of $[PEtPh_3]_2[Ni(Se_4)_2]$, in which there is a crystallographic center of symmetry and thus only four distinct selenium sites.[3]

Table 8. ^{77}Se Solid-State NMR Isotropic Peak Positions for $[Et_4N]_2[M(Se_4)_2]$ Complexes

complex	δ_{iso}/ppm							
$[Et_4N]_2[Cd(Se_4)_2]$	639.8	626.0	595.1	568.4	131.2	64.1	48.1	45.9
$[Et_4N]_2[Hg(Se_4)_2]$	639.8	615.3	571.6	563.1	157.9	90.7	68.3	53.4

The spectra of the zinc and the cadmium complexes both have narrower peaks than that of the mercury complex shown in Figure 4; their peak widths at half-height are 50 and 75 Hz, respectively. In the case of $[Me_4N]_2[Zn(Se_4)_2]$, weak satellites to each peak with a separation of $J \sim 160$ Hz are observed, and these are attributed to J-coupling between ^{77}Se nuclei. It is probable that these correspond to a two-bond J-coupling, as it is commonly found that such coupling values for selenium rings and chains are greater than single-bond values, probably due to greater interactions between the p lone pairs of the Se atoms in question.[16,17] Coupling between ^{77}Se nuclei is probably not resolved in the other samples due to the slightly greater peak widths in their spectra. The cadmium complex shows satellites with $J \sim 290$ Hz for those sites directly bonded to the metal due to coupling to either ^{111}Cd or ^{113}Cd.

Spectra were also obtained on $[Et_4N]_2[Hg(Se_4)_2]$ and $[Et_4N]_2[Cd(Se_4)_2]$ to investigate the extent to which the cation affects the $[M(Se_4)_2]^{2-}$ geometry. The isotropic peak positions are given in Table 8. The spectra have rather worse signal-to-noise ratios than those of the $[Me_4N]^+$ complexes studied; this is because the $[Et_4N]^+$ complexes have shorter ^{1}H $T_{1\rho}$ relaxation times, which means that complete magnetization transfer from ^{1}H to ^{77}Se

(16) Eggert, H.; Nielsen, O.; Henriksen, L. *J. Am. Chem. Soc.* **1986**, *108*, 1725.
(17) Laitinen, R. S.; Pakkanen, T. A. *Inorg. Chem.* **1987**, *26*, 2598.
(18) Adams, D. M. *Metal-Ligand and Related Vibrations*; Edward Arnold Ltd.: London, 1967.
(19) Barrie, P. J.; Clark, R. J. H.; Withnall, R.; Kanatzidis, M. G. Unpublished work.

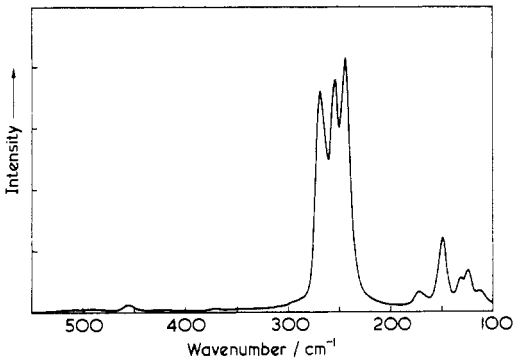

Figure 5. FT Raman spectrum of $[Me_4N]_2[Cd(Se_4)_2]$ as a powdered solid at room temperature over the range 100–550 cm^{-1}.

during CP is not possible. Because of the lower signal strength, the spinning sideband intensities were not analyzed. We also attempted to record spectra on some $[Ph_4P]^+$ complexes, but these samples had very large ^1H spin–lattice relaxation times, which meant that the recycle delay needed between scans for relaxation was too long to give acceptable spectra in a reasonable period of time. The large relaxation times for the $[Ph_4P]^+$ complexes presumably reflect the lack of mobility of this cation in these salts (the ^1H T_1 values are greater than 1 min). It is likely that methyl group rotation, causing efficient ^1H spin–lattice relaxation, persists even in the solid state in the $[Me_4N]^+$ and $[Et_4N]^+$ complexes.

The FT Raman spectra of the complexes display several weak/medium bands attributable to $[Me_4N]^+$ and the presence of DMF. Strong bands at 269, 254, and 244 cm^{-1} in the FT Raman spectrum of $[Me_4N]_2[Cd(Se_4)_2]$ (see Figure 5) lie in the region anticipated for Se–Se stretching modes of the Se_4^{2-} anion, although the possibility that they are due to Cd–Se stretching modes cannot be ruled out.[18] Analogous strong bands at 275, 265, and 254 cm^{-1} are seen in the Raman spectrum of $[Ph_4P]_2[Sn(Se_4)_3]$ and are similarly assigned to ν(Se–Se).[19] The bands at 456, 172, 149, and 124 cm^{-1} have not been assigned. The first may be due to the $[Me_4N]^+$ ion whereas the others could arise from deformation modes of the $[Cd(Se_4)_2]^{2-}$ anion. Attempts to obtain the FT Raman spectra of the zinc and mercury analogues were not successful, giving bands at 235 (vs) and 142 cm^{-1} and to weaker bands at 458 and 440 cm^{-1}, which are very close to the literature values for the two fundamental and two overtone bands, respectively, of trigonal selenium.[20]

Discussion

It is interesting to compare these NMR results with those on $[M(Se_4)_2]^{2-}$ anions in solution measured by Ansari *et al.*[3] In solution, only two ^{77}Se NMR resonances are observed because there is rapid fluxional exchange between different ligand conformations (e.g. between envelope and half-chair conformations), and so only an average chemical shift (and J-coupling) is observed. A comparison of the average values for the ring and metal-bound distinct sites in the solid and the solution NMR values is given in Table 9. It is apparent that the chemical shifts in the solid state and in solution are fairly similar. It is worth noting that these results for the metal-bound selenium nuclei in the solid complexes studied confirm the unusual behavior reported by Ansari *et al.*[3] for the chemical shifts of selenium bonded to d^{10} metal species. In MSe_n rings with M = Mo, W, Ni, Pd, or Pt, the metal-bound selenium typically resonates in the range 500–1100 ppm[2] (depending on ring size and metal) in contrast to the 30–142 ppm observed here. The most likely explanation for this large difference is that there is sufficient electron donation from the metal-bound selenium atoms to those transition metals with vacant d orbitals to cause significant deshielding of the ^{77}Se nucleus. This cannot occur for selenium bonded to d^{10} species, which therefore have metal-bound ^{77}Se resonances to lower frequency than those of the ring selenium nuclei. A similar trend has also been found for ^{77}Se bonded to metals in 2-selenoxo-1,3-diselenole-4,5-diselenolate complexes.[21]

Table 9. Comparison of the Average Isotropic Solid-State NMR Chemical Shifts for the Ring and Metal-Bound Selenium Sites with Solution Chemical Shifts

	solid		solution[a]	
anion	cation	$\langle\delta_{iso}\rangle$/ppm ring, metal	cation, solvent	δ_{iso}/ppm ring, metal
$[Zn(Se_4)_2]^{2-}$	$[Me_4N]^+$	640, 118	$[Ph_4P]^+$, DMF	598, 127
$[Cd(Se_4)_2]^{2-}$	$[Me_4N]^+$	629, 88	$[Ph_4P]^+$, DMF	608, 62
	$[Et_4N]^+$	607, 72		
$[Hg(Se_4)_2]^{2-}$	$[Me_4N]^+$	619, 67	$[Et_4N]^+$, DMF	594, 76
	$[Et_4N]^+$	597, 93		

[a] Solution NMR data taken from ref 3.

While the NMR results for the solid state and for solution are fairly similar, it is likely that the solution chemical shifts are significantly affected by temperature and choice of solvent. On the other hand, the absence of any motional processes in the solid state means that the chemical shifts are highly sensitive to the geometry of the MSe_4 rings. These results show, perhaps surprisingly, that the exact geometry of the MSe_4 rings in the solid is affected not only by the metal center but also by the cation present. In the light of these comments, it is perhaps unsurprising that there is no obvious trend in ^{77}Se chemical shifts for $[M(Se_4)_2]^{2-}$ anions down the M = Zn/Cd/Hg triad.

It is also pertinent to note that the ring and metal-bound sites in the solid may be distinguished not only by their isotropic chemical shifts but also by their shielding anisotropy. The values of $\Delta\sigma$ and η for the ^{77}Se sites in ring positions are similar to those in the other ring positions (for a given metal), and those in metal-bound sites are similar to those in the other metal-bound sites. There is a change in $\Delta\sigma$ and η values for different metals, though it still remains the case that η for the metal-bound sites (range 0.62–0.96) is always larger than for the ring sites (range 0.16–0.61). In principle, the shielding tensor components provide detailed information about the local geometry of each selenium site which may be related to the precise structure of the solid. However, there has thus far been so little ^{77}Se NMR work on solids that it is premature to draw conclusions from the values obtained.

Acknowledgment. The solid-state NMR spectra were obtained on the University of London Intercollegiate Research Service (ULIRS) instrument at University College London. M.G.K. acknowledges financial support from the National Science Foundation for a presidential young investigator award, CHE-8958451.

Supplementary Material Available: Tables giving crystal data and details of the structure determination, hydrogen atom coordinates, anisotropic thermal parameters, and a comparison of calculated and observed powder X-ray diffraction patterns for $[Me_4N]_2[Hg(Se_4)_2]\cdot 0.5DMF$ (3 pages). Ordering information is given on any current masthead page.

(20) Lucovsky, G.; Mooradian, A.; Taylor, W.; Wright, G. B.; Keezer, R. C. *Solid State Commun.* **1967**, *5*, 113.

(21) Matsubayashi, G.; Yokozawa, A. *Inorg. Chim. Acta* **1993**, *208*, 95.